Applied Energy 352 (2023) 121898

Contents lists available at ScienceDirect

Applied Energy

journal homepage: www.elsevier.com/locate/apenergy

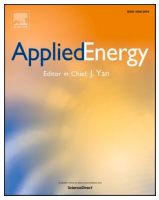

Advances in benchmarking and round robin testing for PEM water electrolysis: Reference protocol and hardware

Thomas Lickert [a], Stefanie Fischer [b], James L. Young [c], Selina Klose [a], Irene Franzetti [a], Daniel Hahn [a], Zhenye Kang [c], Meital Shviro [b,c], Fabian Scheepers [b], Marcelo Carmo [b,d], Tom Smolinka [a], Guido Bender [c], Sebastian Metz [a,*]

[a] Fraunhofer Institute for Solar Energy Systems ISE, 79110 Freiburg, Germany
[b] Forschungszentrum Jülich, GmbH, IEK-14: Electrochemical Process Engineering, 52425 Jülich, Germany
[c] National Renewable Energy Laboratory (NREL), Golden, CO 80401, USA
[d] Nel Hydrogen, 10 Technology Drive, Wallingford, CT 06492, USA

HIGHLIGHTS

- A detailed measurement protocol for PEM water electrolysis is developed.
- A test cell for harmonized measurements in non-harmonized test benches is presented.
- For a set of CCM and PTLs, in-house and across-sites reproducibility is quantified.
- Reference polarization curve data and impedance spectroscopic data are presented.
- Differences in conditioning behavior and thermal management are analyzed.

ARTICLE INFO

Keywords:
PEM water electrolysis
Harmonized test protocol
Benchmarking
Reproducibility
Conditioning of catalyst coated membrane
AFC TCP Task 30

ABSTRACT

While the number of publications in the PEM water electrolysis community increases each year, no common ground concerning reference hardware (test cells and test bench) and testing protocols has been yet established. This would, however, be necessary for the comparability of experimental results. First attempts for such reference hardware and procedures have been made in the framework of the Task 30 Electrolysis within the Technology Collaboration Programme on Advanced Fuel Cells (AFC TCP) of the International Energy Agency (IEA). Since then, improvements of both the test hardware (test cell and components) as well as the measurement protocol were identified, and a revised methodology and key results based on a comprehensive measurement series have been obtained. A detailed protocol for testing commercial reference components with a reference laboratory test cell developed in-house by Fraunhofer ISE is presented. For evaluation of the protocol and the hardware, it was tested at three different institutions at the same time. Impedance spectroscopic and polarization data was acquired and analyzed. The obtained differences in performance were calculated to give the community an expectation window to compare own data to. Finally, the importance of a thorough temperature control and the conditioning phase are demonstrated.

1. Introduction

Polymer electrolyte membrane water electrolysis (PEMWE) will experience a rapid market ramp-up in the future as green hydrogen will play a key role in transforming the energy system towards a carbon free system [1–4].More and more companies, universities and scientific groups are producing a large amount of data on different kinds of test cells, stacks, assembled with all kinds of components and materials [5]. A comprehensive review on early works in PEMWE is given in the works of Carmo et al. [6]. Since then, numerous further works with different hardware and test conditions have been published [7–16]. More than ever, harmonization and benchmarking activities are crucial to make group to group comparisons possible and increase the trust that literature results are reproducible and accurate.

* Corresponding author.
E-mail address: Sebastian.metz@ise.fraunhofer.de (S. Metz).

https://doi.org/10.1016/j.apenergy.2023.121898
Received 31 May 2023; Received in revised form 1 August 2023; Accepted 2 September 2023

Since the last publication by the Task 30 Electrolysis benchmarking group [16] of the AFC TCP, significant improvements in cell performance [5,7,17–21], catalyst systems and loadings [19,20,22–31], porous transport layers (PTLs) [32–37] and durability have been reported [9,11,38].

Iridium and platinum are still the most wildly used catalysts and hence gold standard in PEMWE. The actual catalyst content is still higher than it would be necessary with optimal catalyst utilization, so numerous research activities have aimed at catalyst reduction while keeping the performance approximately unchanged. [19,20,22–31] As especially iridium is scarce and expensive novel catalyst concepts as supported catalysts [23,25,39] or more advanced structures, such as the Sr_2CaIrO_6 mixed oxide, are of great interest. Sr_2CaIrO_6 possesses sacrificial components, such as Ca or Sr, which leach out during operation and cause a strong reconstruction of the catalyst layer (CL) [40].

On the other side of the interface, the PTLs and their contact with the CLs are decisive for performance and durability [11,22,37,40]. Increasing current density causes significant performance loss due to dry-out and oxygen saturation. [22] Therefore, modifying the structure and composition of the PTL has become another area of interest for the researching community. Various treatments have been studied, such as the effect of titanium hydride formation on performance and durability or classical etching to remove surface passivation [37]. Similarly, laser ablation has been used to improve the contact between the patterned PTL and the lightly loaded CL [41]. For an improved CL-PTL interface, these two components can no longer be developed independently, an approach that is only in its infancy so far. In any case, there is a tendency to reduce the thickness of the PTL.

While the above mentioned advanced systems show individual successes, a unifying element connecting these results is missing [42] as cell hardware [21,26,28,43–49], cell components [18,27,28,49,50], conditioning procedures [16,28,51,52] and testing protocols [16,52–56] differ considerably. As a result, it is still nearly impossible to comparatively evaluate results from different working groups on PEM water electrolysis, despite the steadily increasing interest and the rapidly growing number of publications on this topic. Tomić et al. [52] address this issue by conducting a comparative analysis and critical review of different proposed degradation protocols, which were experimentally validated to provide a better basic understanding. They also confirmed the urgent need for harmonized testing protocols, especially for the initial period, called conditioning. Moreover, various national funding agencies as the European Commission, the Department of Energy (DOE) in the USA or the German Federal Ministry of Education and Research have also recognized this shortcoming and do support the development of harmonized test protocols, to enable better benchmarking of project results. However, these efforts are still in their infancy and comparable results are not yet available or published. Recently, the European Joint Research Centre (JRC) has described detailed individual procedures which can be used to set up a measurement protocol with harmonized terminology [54,57,58] for all main low temperature technologies of water electrolysis. Among other things, certain test conditions, design of hardware, number and positions of sensors, their measurement accuracy and analysis routines for important characteristic values are proposed. This very comprehensive conception is based on the experience of the participating industry and research institutions but can only be understood as a starting point for harmonization, since application in practice is lacking so far and no comparative measurements have been carried out or published yet. A detailed, internationally applied, and harmonized reference measurement protocol is still not published, nor has it been critically experimentally evaluated.

With the continued work of our benchmarking group within the Task 30 of the AFC TCP, we aim to further the discussion on harmonization of testing protocols and hardware. For improvement, a significant effort should be placed on (i) identifying an open-source cell hardware that can serve as a reference system, and (ii) defining test conditions and protocols. The first will enable to connect results from various institutions that were measured with their own hardware as long as one validated measurement with the reference hardware exists. The second will generally improve the reproducibility of creating experimental results in general. Both together would enable the meaningful comparison across the entire PEMWE research community and help to bridge the "valley of death" between academic research and industrial application [59].

The participating institutions of this contribution evaluated the method and the system, defined the reference cell components, and developed a harmonized testing procedure. The used test cell is currently available through Fraunhofer ISE. The cell components, like catalyst coated membranes (CCMs) and PTLs, which together form the membrane electrode assembly (MEA), are commercially available. The overall objective of this work is to present this potential reference measurement method, the reference hardware system and give the PEM water electrolysis community expectation values for performance, reproducibility, and variation to other groups, that can be expected.

2. Experimental setup

To understand the choices made in the process of developing a reference protocol for PEM electrolysis, a good understanding of the underlying principles is essential. Describing these underlying principles comprehensively and to a level of detail they deserve goes beyond of this article. We strongly encourage the reader to consult some of the excellent descriptions of fundamental processes already available in the literature [6,9,60–65]. Together with the measurement protocol to be used, the experimental hardware setup is one of the key challenges in a round robin benchmarking exercise. One of the decisions to be taken is which hardware needs to be identical for all partners and which hardware differences need to be accepted. It is obvious, that the test cell as well as the components need to be harmonized, as differences can have a high impact on the measured results. For the test bench hardware, it needs to be accepted that this is and will always be to a certain extent different between different groups.

2.1. Test cell

For this benchmarking activity a 4 cm^2 test cell previously developed by Fraunhofer ISE within a project financed by the Federal Ministry of Education and Research of Germany in the framework of Power-MEE (03SF0536E) was employed. As shown in Fig. 1a, the cell is housed in a compression cage which contains a centered screw for applying a variable compression force to the cell. The applied forced is monitored with an integrated force sensor (K-K14/N410-G25 sensor, Lorenz Messtechnik GmbH, Germany) during assembly, start up and operation (Fig. 1a). The anode and cathode compartments of the cell feature Polyetheretherketone (PEEK) frames which hold the PTL and determine PTL compression (Fig. 1b). To seal the cell, Fluoroelastomer (FKM) based flat sheet sealing (Freudenberg, IceCube, 60 FC-FKM 200) is used. The parallel flow field of the cell is shown in Fig. 1b. It consists of 10 channels with a width and depth of 1.0 mm. The channels are separated from each other by 9 land sections which have a width of 0.9 mm. The entire flow field is encased by a 0.9 mm land section. To run round robin tests with PTLs that provide reproducibility on an industrial standard, laser cut titanium felts with 1 mm thickness from Bekaert (2GDL40–1,0), sputtered with platinum on both sides (more information in Section 2.2) were used.

The thickness tolerances of both, the PTLs and PEEK frames reached up to +60 µm. This significant variation was mitigated by determining the exact thickness of the PTL and pairing it with a specific pocket depth of the PEEK frame (Fig. 1c). For all cells operated in this work, the overstand of the PTL over the height of the measured pocket depth was adjusted to 70 µm ± 10 µm. A detailed description of the adjustment process is given in the supplementary data. A similar approach was published by Martin et al. [43]. To warranty small and reproducible

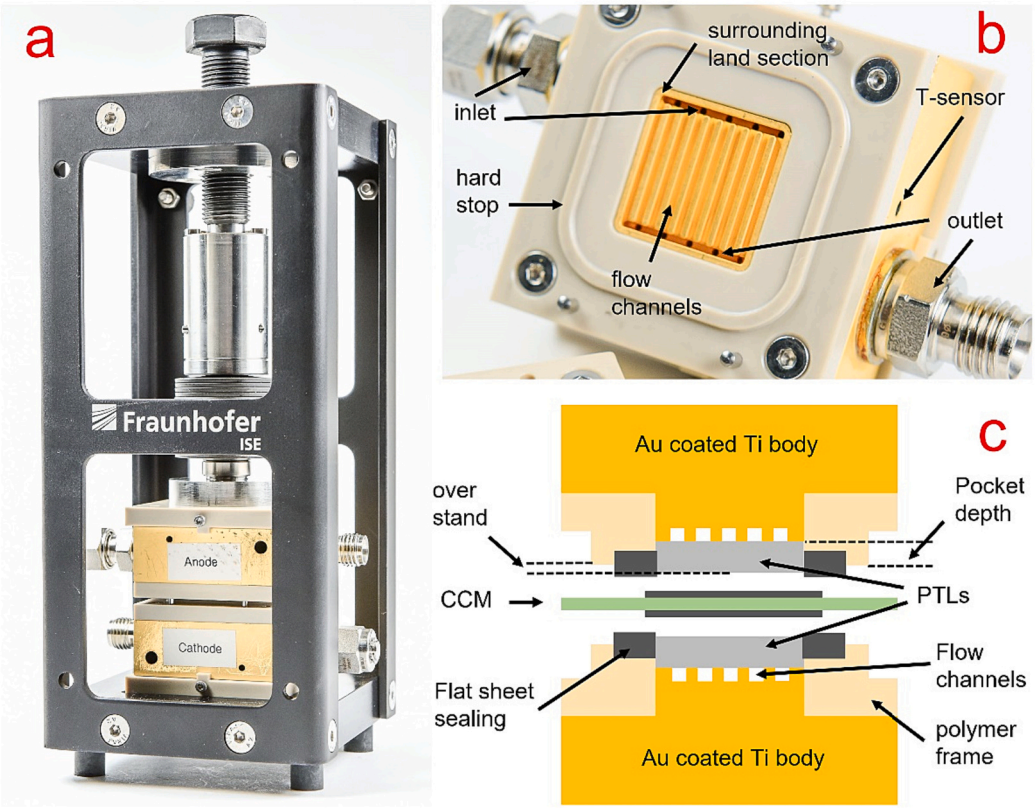

Fig. 1. Compression cage with test cell in it (a), details of a single half cell (b) and schematic of the test cell setup (c).

contact resistances between the titanium base material of the flow-field and the PTL, a gold coating on top of a thin contact layer of platinum for better adhesion was applied. For electrical contacting to current lead and voltage sense cables, each flow field block contains holes for a 2 mm and a 4 mm banana plug connector.

An additional 2.1 mm hole is provided to position a temperature sensor at a position close to the electrochemical reaction in 4 mm distance to the lower edge of the flow field, so that temperature changes can be detected as fast as possible. The fluidic connections are realized by a G1/8 in. thread with a length of 7 mm.

2.2. Cell components

This section includes the components and materials used to collect the data for the herein described study. A description of state-of-the-art materials and components with latest references are described in Section 1.

PTLs: The PTL materials consist of titanium felts with 1 mm thickness from Bekaert (2GDL40–1,0), coated inhouse on both sides at Lab 3 and used on the anode side as well as the cathode side. The titanium felts were cut to size using a MiniLase™ Auto Door laser marking system to fit the sample compartment. After removing burrs from the cut PTL samples and smoothing of the edges, the PTL materials were ultrasonically cleaned: in acetone, isopropanol, ethanol, and finally in deionized (DI-) water for 10 min each. Self-heating of the ultrasonic resonator leads to increasing temperatures during cleaning, but always remained below 60 °C. At the end of cleaning, the materials were rinsed in DI-water and allowed to air dry (more details in the supplementary data). Next, the titanium felt PTLs were sputter-coated with platinum on both sides. This Pt coating was applied using a custom sputtering system in Lab 3. After the samples were placed in the sputter coater, the chamber was evacuated to a base pressure of ~6.7E-9 bar (~5E-6 Torr). Argon gas (UHP 99.999% Ar gas) was supplied at approximately 15 sccm (standard cubic centimeter per minute) to establish a setpoint chamber pressure of ~1.3 E-5 bar (10 mTorr). The sputtering power setpoint was 20 W yielding a current of about 70 mA. A sputtering break-in time of two minutes was allowed before opening the shutter to commence deposition. The same process was repeated for each sample side. The deposition time was 15 min to yield a Pt loading of approximately 0.1 mg*cm^{-2} as measured by x-ray fluorescence (XRF) spectroscopy (Fischer XDV-SDD).

CCMs: A commercial three-layer CCM from Greenerity, using a Nafion® 115 membrane, a Pt-based cathode and an IrO_2-based anode was used. Within the actual measurements, fully coated CCM sheets were used, cut to size, and distributed between the labs. In the cell setup, the flat sheet sealings of cathode as well as anode were hence in direct contact with the catalyst layers of the CCM. While this might cause some longtime effects in electrolysis stacks on the industrial scale, no issues were observed with this approach throughout the measurements reported in this paper. For reproducibility and contact resistance reasons, the cells were assembled with dry CCMs, and the humidification and swelling of the latter happened during the conditioning phase.

For details on the material preparation and cell assembly, the reader is referred to the supplementary data.

2.3. Test benches

As mentioned in the test cell section, harmonization efforts concerning hardware are limited to the test cell and test cell components (PTL, CCM, coating). Harmonization of test benches across the wider community is rather hard to realize and hence was deliberately not attempted within this study. It was rather the intention to check, how and to what extend harmonization can be achieved with conceptionally different test benches and lab environments. Two conceptually different test benches are depicted at the beginning of the supplementary data.

Test benches can be set up simply from scratch with standard piping and process control. The advantage of these test benches is that they can easily be adapted to a specific operation mode. Test benches that can be bought are usually more potent, but can be complex to operate and the

option of adaption is more limited. In that respect, some differences within the test bench setup were accepted on purpose for this contribution to reflect the reality in the scientific community. Major differences are:

- Water feed: Lab 1 and Lab 2 recirculate DI-water once it passed through the cell flowing through an ion exchanger resin to stabilize water conductivity below the required value (< 1 µS*cm^{-1}). Lab 3 uses the so-called single pass mode. DI-water passes through the cell and flows to the drain after leaving the test cell.
- Water conductivity: At Lab 2, the conductivity of the DI-water is continuously controlled by sensors inside the gas-water separators, whereas at Lab 1 it is only checked before and after each test. At Lab 3 conductivity is defined by controlling the input water stream.
- Pressure control and differential pressure: One of the labs is located at higher altitude, and therefore the environment is at lower pressure. Backpressure valves are used to increase pressure values to sea level. At another lab, located almost on sea level, a slight overpressure at the cathode is needed for process control reasons and hence a small differential pressure is generated. At the third lab, both sides are open to the environment and the lab is located almost at sea level.
- Electronics: All three partners use different electronic loads and different frequency response analyzers (FRAs). Resulting differences in e.g. cable inductivities, measurement precision or simply the necessity of changing cables during tests to be able to use the devices makes it a generally underestimated influence on measurement data. The test protocol that was developed and is published with this contribution copes with this by introducing so called down times. A more detailed description of the protocol is explained in Section 3. A description of the electronic hardware that was used is given in Section 2.3.2.
- Dynamic of heat source: Across the three labs, different heat sources were used. At Lab 1, two thermostats with individual water baths, pumps and heating loops are used and are connected to heat exchangers that transfer the heat to the fluidically decoupled reactant water circle. The other two labs use resistive heating solutions directly applied to the reactant water tube. At Lab 2, a metallic heat block, which the tube is integrated in, is heated electrically. At Lab 3, a resistive heat tape is wrapped around the tubing and heated electrically. Thermal dynamics are therefore higher for at Lab 2 and Lab 3.

2.3.1. Thermal management of anode and cathode

The temperature has a major effect on the performance of an electrolysis cell and even small temperature changes can have an impact. Therefore, precise control of the temperature inside the cell is mandatory for reproducibility. As the test cell used in this study doesn't provide the option of external heating (e.g. by a separate heating loop or a heat patch on the cell body), preheated fed water is used for temperature control. As the Joule heat generated inside the cell and the amount of thermal losses (i.e. thermal radiation of the cell to the surrounding air) can vary depending on the current density, a feedback loop based on the measured temperature of the cell has been implemented at all three labs. For most of the current densities, there is a temperature gradient across the test cell, such that the position of the temperature sensor is an important question that needed to be addressed for establishing a reproducible measurement protocol. Ideally, the herein presented setup should have 6 temperature sensors (Fig. 2) of which one on the anode and one on the cathode side needs to be chosen as temperature regulation point. Of the nine possible combinations, the following four variations were tested:

- Variation 01: Anode internal (T1); Cathode internal (T2)
- Variation 02: Anode internal (T1); Cathode inlet (T4)

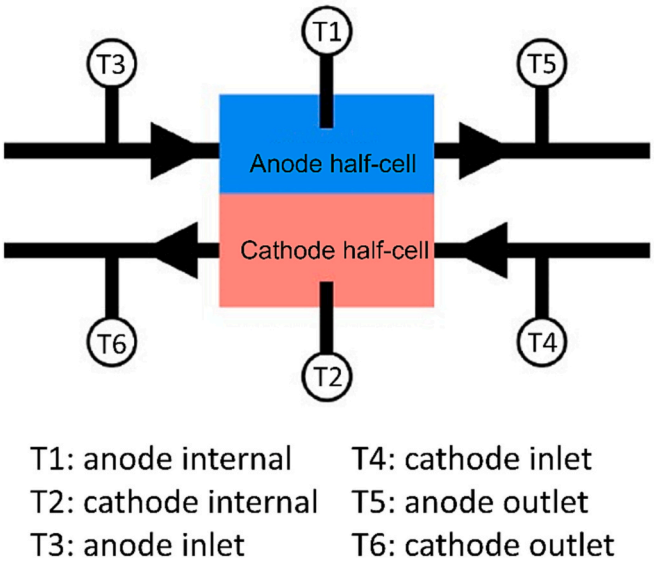

Fig. 2. Positioning of the six temperature sensors in the two independent half-cell loops.

- Variation 03: Anode inlet (T3); Cathode inlet (T4)
- Variation 04: Anode outlet (T5); Cathode outlet (T6)

On the first glance, Variation 01 would be considered as the most reproducible set-up, as the position of the temperature sensor inside the cell would be defined to the highest level of harmonization: It would be identical for all partners. However, not for every test bench the integration of a Pt100 temperature sensor to be used as temperature control point can easily be done. In fact, Lab 2 had to integrate the temperature sensor of the test bench into their cell and for Lab 3, it wasn't possible to integrate all the 6 sensors. As it was realized, how complicated the usage of Variation 01 might turn out in the laboratory, additional variations with temperature sensors being implemented close to inlet/outlet on the anode/cathode side were tested. Lab 3 recorded Variation 02 for all measurements, herein as a control case for the other labs that varied their temperature regulation points.

2.3.2. Electronic hardware

Electronic devices might even be more diverse than test benches throughout the community. Results from an internal survey conducted by Fraunhofer ISE, during an impedance workshop, revealed that ten different suppliers for impedance hardware cover a large part of the community (based on the limited number of participants at the workshop). For direct current (DC) power supply, the number is probably even higher. Due to this variety, and the differences that come along with hardware differences, e.g. test bench operation or data acquisition, a measurement protocol that is as universal as possible, should cope for this, to be applicable by as many groups as possible. For the herein described electrochemical tests, three different electronic setups are used and listed in Table 1.

3. Test protocol / methodology of characterizing test cells

Unlike the field of PEM fuel cells, where a measurement protocol is available based on work coordinated by the DOE [66,67], no such precise and validated protocol exists for PEM water electrolysis. The JRC has compiled comprehensive documents on measurement procedures and terminology [54,57,58] which have been collated from the experience of several industrial partners and research institutions. As part of the work, a test procedure for a stepwise ascending and descending polarization curve in galvanostatic mode is presented in [57] but the

Table 1
List of the used electronic devices by the three contributing partners.

Device	Lab 1	Lab 2	Lab 3
DC power supply	Zahner PP241	Sorensen XTR 6–110	HP 6031A
Voltage measurement	Zahner Potentiostat (PP241)	Sorensen XTR 6–110	Keithley Model 2000
Impedance device	Zahner Zennium Pro	Biologic HPC-1005	Autolab Metrohm PGSTAT 302 N
Current booster	Power Potentiostat (Zahner PP241)	100A Biologic HCP-1005 booster	20 A Autolab Metrohm booster
Software (electronic control & data recording)	In-house developed LabView VI	HyWARE II (Greenlight Innovation)	Multiscan (Grandalytics)
Software (process control		HyWARE II (Greenlight Innovation)	In-house developed LabView VI for back pressure valves

protocol allows a considerable degree of flexibility, prone to different ways of adaption, potentially leading to different results. Hence, it could be considered only as a starting point for harmonization and – even more important - its practical application and comparative measurements are lacking so far. A fully harmonized and tested reference measurement protocol is still not published. It should be emphasized, that setting up such a general test protocol is a tremendous task and is not provided in the actual publication, either. What we do provide is a detailed, harmonized protocol that has survived the practical trial in three individual groups, coordinating their work within the framework of their partly non-harmonizable test hardware, meaning test bench and electronics (see Section 2).

3.1. Impact of non-harmonizable hardware on the test protocol

The testing protocol used is based on the experience of the participating institutions and includes several compromises to perform the same measurements. In the practical testing, as already in our first Round Robin tests [3], the temperature control proved once more to be one of the key issues. Analysis went so far as to check the influence of the positioning of the temperature sensor that controls the water circuit temperature on anode/cathode side either at the inlet pipe, the outlet pipe or inside the cell (see Section 2.3.1). A second major impact originates from the used electrical hardware (see Section 2.3.2): While some electrical devices can measure both, polarization curves as well as electrochemical impedance spectroscopy (EIS), others use difference devices for these measurements. Hence in the test protocol, these measurements had to be decoupled to allow one of the participating partners to change the hardware by hand. Also, the heating and cooling rate to adjust to the two different temperatures are different and depend on the test bench and/or the lab environment (exposure to sunlight or air exchange rates). To address the latter two points and to keep the protocols synchronized at the same time, an extra downtime of one hour was added in several parts of the test protocol, see Section 3.2).

3.2. Test protocol description

The formal steps for the test protocol used are shown in Fig. 3. Although not usually discussed in detail, preparation is a critical part. It includes selecting the PTL (which needs to fit the pocket depth of the test cell, see Section 2.1), flattening the surface and/or edges with sandpaper, and properly cleaning the surface and test cell. To ensure the highest level of reproducibility for each cell that was assembled, a fresh set of PTLs, on anodic and cathodic side, was used to have comparable states of the PTLs at beginning-of-test. For some CCMs, it is recommended to pre-swell them in water before putting them into the cell, for some others, this can lead to an excessive wrinkling which could even

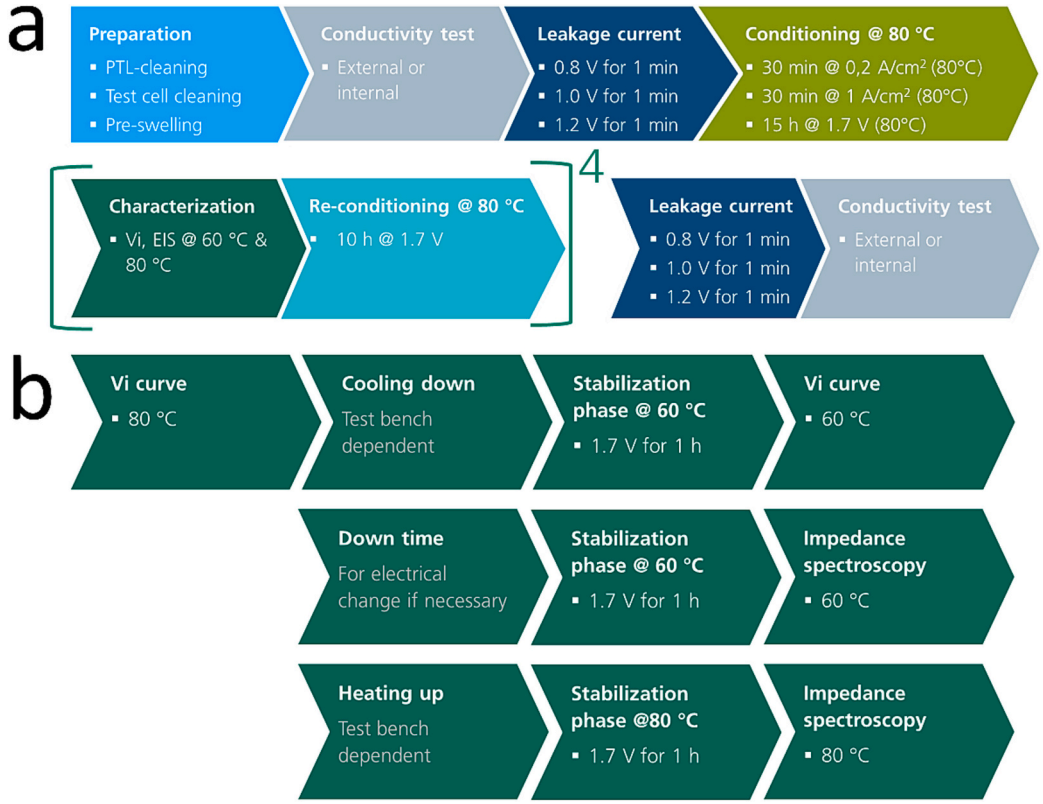

Fig. 3. (a) General test script with iterated Characterization/*Re*-conditioning loop and (b) individual steps within the Characterization.

lead to delamination of the catalyst layer [29,68]. In the actual case – and unlike earlier attempts – the cell was assembled using a dry, not pre-swollen CCM. By this approach, the membrane predominantly swells in the axial direction and performance data indicate that no delamination is occurring inside the cell. In the next step, the cell is heated up to $T = 80$ °C and the temperature was held for $t = 60$ min. Afterwards, the conductivity of the used water is tested (for those labs that do not have an in-line check of the water conductivity) to avoid performance differences due to contaminations. Values that must be achieved can be found in the detailed description of the protocol in the supplementary data. Next, a current leakage test is performed at three different voltages: 0.8 V, 1.0 V and 1.2 V. This is done, to determine, that there is no short circuit, e.g. caused by one of the PTL-fibers or burrs from the cutting process of the PTLs, that could penetrate the CCM. After these two quality control steps, the first conditioning is started with two galvanostatic steps for 30 min each at 0.2 A/cm^2 and 1 A/cm^2, respectively and a potentiostatic step for 15 h at 1.7 V. With the first, galvanostatic steps of the conditioning, we followed the suggestion of the CCM producer. The following potentiostatic mode allows to control any free energy driven surface change mechanisms. We, however, identified that when following this procedure, the CCMs are not fully conditioned at the beginning of the test. Hence the extension of the time at 1.7 V.

The tested temperatures, pressure and water flow rate for the performance and reproducibility evaluation, has been chosen to cover state-of-the art and future operating conditions in industrial PEM water electrolysis systems. For the temperatures, 60 °C is widely used in the industry and therefore usually used as a reference temperature [54], 80 °C is aspired for the next years [4]. The pressure is chosen to meet the requirements for most of the scientific groups. The flow rate was chosen according to the channel structure of the used test cell to suppress mass transport limitation with the used MEA and PTL combination.

The characterization phase begins with the measurement of the polarization curve at 80 °C - the temperature, the conditioning temperature, such that no temperature adjustment is necessary between these two steps. First, the different measurement points of the polarization curve are measured in the order of an increasing current density ("up-curve"). Afterwards, the same points are measured, but with opposite order, i.e. in the order of a decreasing current density ("down-curve"). After this step is finished, the temperature needs to be lowered to 60 °C, hence a cooling down time is required, the duration of which depends on the test bench. To mitigate this test bench dependent difference of the colling down time, an additional stabilization phase (1 h at 1.7 V) of one hour was added, after which the polarization curve is measured.

With the same rationalization (no change in temperature to the previous step), the EIS spectra were first measured at 60 °C. Before this was possible, Lab 2 had to manually adjust the electronic hardware connections. To compensate for potential effects this voltage/current disruption might have on the EIS spectra to be measured, another stabilization phase (1 h at 1.7 V) was run. This was done at all sites to keep the protocol as harmonized as possible. The EIS spectra (also in the later step at 80 °C) were measured at five different current density points (0.1; 0.5; 1.0; 2.0 and 2.5 A*cm^{-2}). After the EIS measurements at 60 °C were obtained, the temperature was increased to 80 °C, with a stabilization phase (1 h at 1.7 V) to compensate for the different heating rates at the different sites. As last step of the characterization phase, the EIS spectra at 80 °C are obtained at the same five current densities as before at 60 °C. With this, the EIS measurements at both temperatures are finished.

The characterization phase is followed by a re-conditioning for 10 h at 1.7 V. The practical reason for this phase was to ensure that there wouldn't be any need for an adjustment of the working hours for the manual changing of the equipment at Lab 2, which is crucial in general, to make such a protocol usable for everyday lab work.

The two phases of characterization and reconditioning were repeated in total 4 times. Depending on the laboratory, this was either done with different temperature control settings (Lab 1 and Lab 2) or with unchanged temperature control settings (Lab 3). Based on these repetitive measurements, it was possible to compare the influence of the repetitions themselves on the one hand and the different temperature control settings on the other hand, see results Section 4.3.

Finally, the two steps of a current leakage test and a conductivity test of the used water are re-run to check whether there have been any changes during the test protocol or not. While two labs have the convenient ability to continuously monitor the water quality (in the test bench or via the house DI-water supply monitoring system), Lab 1 is lacking this ability and can only confirm the water quality during the run in an a posteriori measurement.

The detailed measurement protocol is available in the supplementary data.

3.3. Analysis of impedance data

By fitting the measured impedance spectroscopic data to an equivalent circuit model, additional insights into the individual loss mechanisms can be obtained [45,69–73] In Fig. 4, an example of the python fit is given for data from Lab 1 (MEA 2, $T = 60$ °C, $i = 1$ A*cm^{-2}) is given. In the actual case, an equivalent circuit with a linear sequence of an ohmic resistance Rm and two parallel arrangements of a constant phase element (CPE1/CPE2) and an ohmic resistance (R1/R2) was chosen and realized by an in-house developed python code. For Lab 2, an additional inductance (La) was included to be able to correctly analyze the data (depicted in the graphs of Fig. 5). The fits were reviewed for their informative value using a chi-square (or χ^2) test (statistical method to quantify the difference between data and the fit) for their real- and imaginary part for all frequencies, which are lower than 2% for all spectra fits ($\chi^2 < 1\%$ for 93% of all frequency points). The upper part (a) shows the Nyquist plot of the data points (blue points, raw data), the individual RC-elements (high frequency part Z_{HF} in red, low frequency part Z_{LF} in green,) and Z_{sum} (purple curve). The data fit is overlapping with Z_{sum} and therefore not seen in Fig. 4. The lower part (b) shows the residuals, meaning the deviation between the fit and data points for both real (blue, ΔRe)- and imaginary parts (orange, ΔIm) for all frequencies.

The main reason for an impedance analysis within this contribution is that it's needed for the iR-correction of polarization data. Herein, high frequency resistances (HFRs) were extracted from the respective Nyquist plots for representative current densities ($i = 0.5$; 1,0; 2,0 and 2,5 A*cm^{-2}) by fitting the data using an in-house developed python code from Lab 1. As limitations of the electronics (sampling precision at low current density) led to insufficient noise levels for the lowest measured

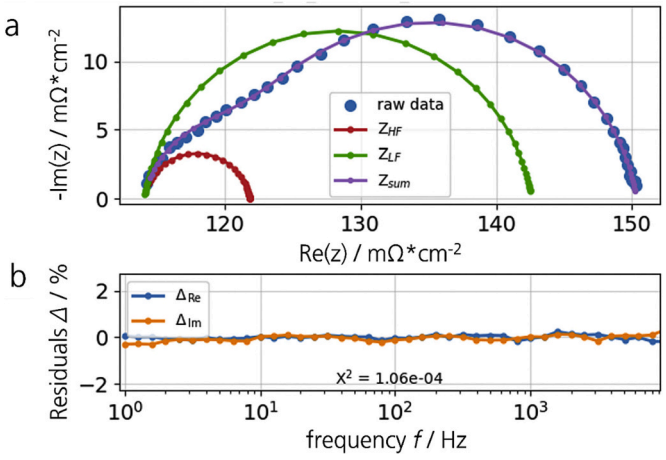

Fig. 4. (a) Example of Nyquist plots with individual contributions for high frequency (red line) and low frequency elements (green line), measurement data (blue points) and the sum of both (purple line). (b) Corresponding differences of data compared to measurement points for real (blue) and imaginary part (yellow). (For interpretation of the references to colour in this figure legend, the reader is referred to the web version of this article.)

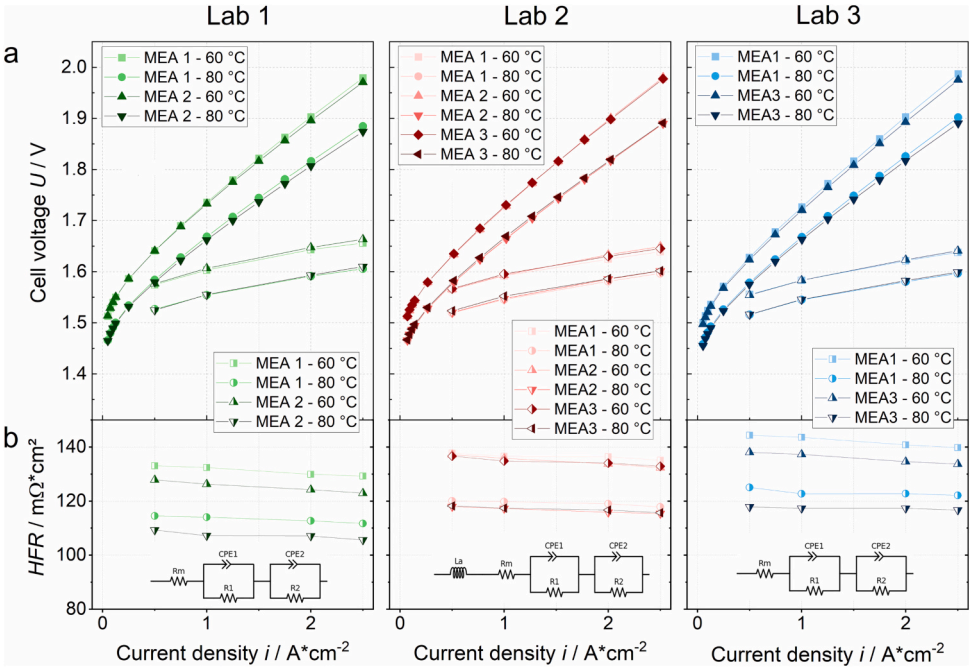

Fig. 5. (a) Polarization curves in uncorrected state (filled symbols) and iR-corrected state (half-filled symbols) for 60 °C and 80 °C and all three labs. (b)Corresponding HFRs, extracted from impedance data and the used equivalent circuits.

current density of 0.1 A*cm^{-2}, the fit and therefore the HFR for 0.1 A*cm^{-2} was not included in the further analysis. The resulting iR-corrected graphs allows the distinction between ohmic and non-ohmic effects.

4. Experimental results and discussion

In the results section, two different types of reproducibilities will be discussed, the "in-house" and the "across-sites" reproducibility. The in-house reproducibility is a measure for the ability at each institution to reproducibly create the same measurement conditions and hence obtaining the same results for the same type of measurements at the specific lab. Especially quality issues with the used materials, or inaccuracies in cell or test bench handling would result in a poor in-house reproducibility. A good in-house reproducibility is easier to obtain, and standard deviation will be lower than for an across-sites reproducibility as for the across-sites reproducibility, the measurement conditions in the cell must be identical at each of the different labs. This is much harder to achieve and took an iterative process to address the non-harmonizable differences originating from different experimental setups (test bench, electronics, laboratory infrastructure) and different working methods to ensure the necessary control parameter were sufficiently controlled at each of the labs. For simplicity reasons, in-house and across-sites reproducibility were obtained from the same data set generated by the test script shown in Fig. 3, which was run for three individual cell assemblies at each lab. For Lab 1 and Lab 3, one of the cell assemblies was taken out of the comparative analysis as test bench interruptions occurred during the measurements, prohibiting the inclusion of this data in the analysis here. Therefore, two cell assemblies for Lab 1 (labelled "MEA 1" and "MEA 2") and Lab 3 (labelled "MEA 1" and "MEA 3" and three repetitions for Lab 2 (labelled "MEA 1", "MEA 2" and "MEA 3") are discussed in the following. For easier reading and comparison, the data is colour coded throughout the entire publication. The data for Lab 1 are shown in green, for Lab 2 in red and for Lab 3 in blue.

4.1. In house reproducibility

The in-house reproducibility is seen as the basis for the later comparison across the labs. Lab specific observations and general data differences must be considered here to understand the data comparison across the labs. In the top part of Fig. 5, the polarization curves for a cell assembly are shown at $T_1 = 60$ °C and $T_2 = 80$ °C together with the iR-corrected curves. At the bottom part, the HFRs for the measured current densities are depicted together with the equivalent circuits that were used to fit the impedance spectra. At the first glance, the measurements show a high reproducibility, but it must be accepted that for the uncorrected cell voltage data, already the in-house comparison (separate consideration of each lab) of the polarization data shows differences in the order of several mV. In general, Lab 2 shows lower differences throughout the entire current density range, than Lab 1 and Lab 3. This is also true for the HFR values. As differences decrease after iR-correction, they mainly originate from ohmic effects. But as differences remain also in the iR-corrected data, kinetic effects must also play a role as the origin, but to a smaller extent than the ohmic effects, see also the more detailed analysis in the sections below. The polarization curves in Fig. 5 show high linearity above $i = 0.5$ A*cm^{-2} for all labs, resulting in the assumption of negligible mass transport losses (MTL).

4.1.1. Results from impedance analysis

For all labs, the impedance spectra for the different measurements described above recorded at 60 °C and different current densities are presented in Fig. 6. The Nyquist plots are used to give the reader an impression of the in-house differences and the differences across the labs that were observed. To make the details easier to recognize, the spectra for low (a) and high current densities (b) are plotted in different figures with different scales.

When analyzing the spectra for high current densities (see Section 3.3 for details) the extracted HFRs show an in-house and across lab shift (see Fig. 6). All labs show a decreasing HFR with increasing current density with impedance differences between 1 and 5 mΩ*cm^2 (for the tested current densities of 0.5 and 2.5 A*cm^{-2}). This is commonly attributed to a heating effect on the anodic side by the overpotential, and a subsequent heating up of the membrane which results in a higher protonic conductivity [65]. Lab 1 and Lab 3 show the steepest slopes (4.5–5 mΩ*cm^2 respectively) and the highest deviation between MEAs (5–7 mΩ*cm^2 for both labs) whereas Lab 2: shows lower slope values

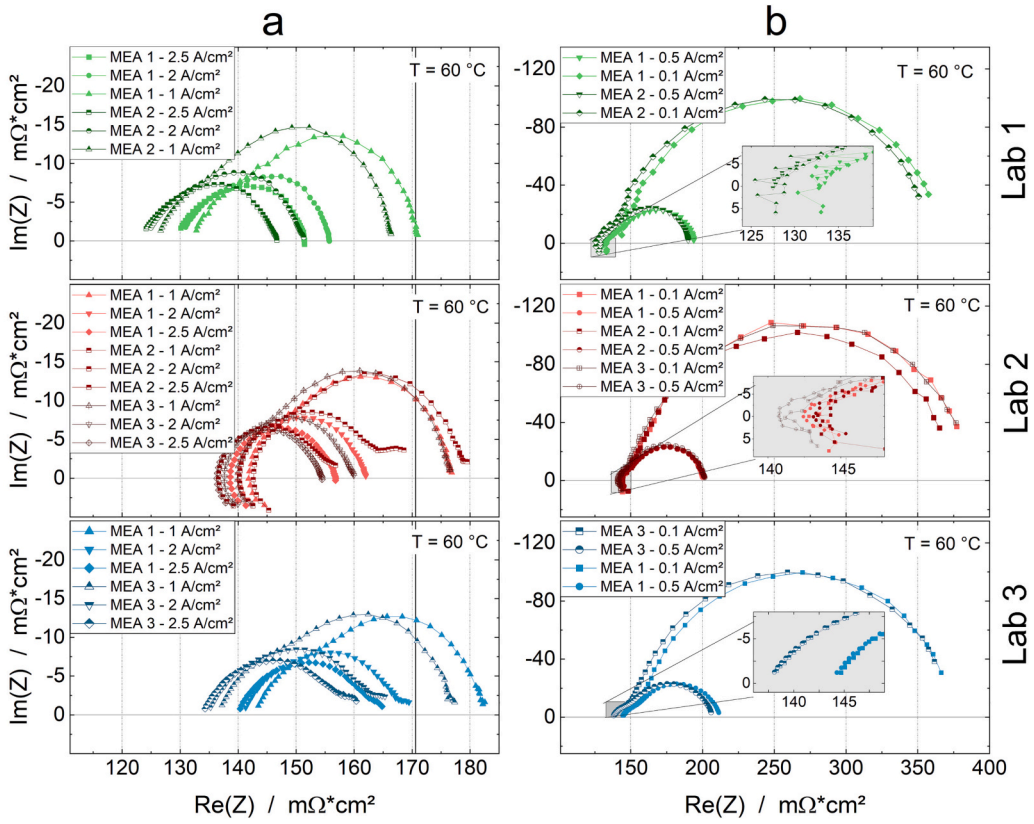

Fig. 6. Impedance data at 60 °C in the Nyquist representation for all three labs, showing (a) data at high current density (1–2.5 A*cm^{-2}) or (b) data for low current density (0.1–0.5 A*cm^{-2}).

(2–4 mΩ*cm^2) and lower deviation between the MEAs (1–3 mΩ*cm^2). Although this contribution is not intended to analyze impedance spectra to a comprehensive extend, there is a deviation from the textbook behavior for some of the measurements observed, which should shortly be addressed. In the high frequency area, there is a deviation from a perfect semicircle and the graphs show a linear section, clearest visible in the graphs of the low current densities. This can be assigned to the limited protonic conductivity in the electrode layer which can be

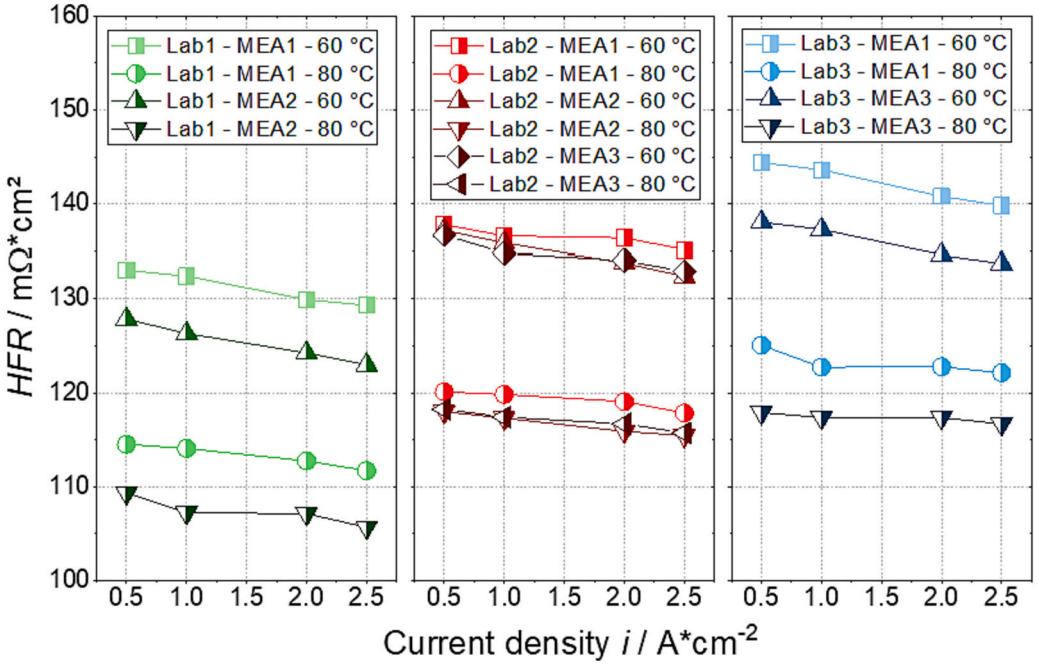

Fig. 7. Averaged HFR at different temperatures, differrent current densities and the different Labs as a measure for the ohmic resistances.

described by the so called "transmission line model" [35]. Or in a simpler approach, by a second parallel arrangement of a constant phase element (CPE) and an ohmic resistance (R), which was used in the presented work, as the effect was not so clear and therefore assumed to be of minor importance for comparable HFR's. In addition, there is a difference in the expression of the respective inductivities. Lab 2 seems to have higher cable inductivities as spectra go further down below the real axis towards higher positive values. These differences, and the resulting changes, are considered by the fit of the spectra [74]. Another noteworthy behavior can be seen at low frequencies but high current densities (above 1 A*cm^{-2}). For these measurements, a second capacitive element appears for MEA 2 at Lab 2 and MEA 1 & 3 at Lab 3. (seen best in Fig. 6 left part). Lab 1 data does not show the effect. Usually, this second capacitive element is attributed to mass transport losses if the effect increases with current density [24]. This mass transport loss is commonly considered to be caused by inhibition of product gas removal – mainly on the anode side [30,38,49,73]. To summarize: Lab 1 shows the lowest ohmic resistances, Lab 3 the highest with the values of Lab 2 in between. This holds true for both 60 °C and 80 °C and representative mean values for each temperature, lab and current density are given in Fig. 7. Differences in performance and the individual losses are more comprehensively visible than in the polarization curves.

4.1.2. Uncorrected and iR-corrected voltage deviations

In this section, the in-house spread of the measured polarization curves for both, uncorrected and iR-corrected voltages, is analyzed. From the Polarization curves in uncorrected and in iR-corrected state, the highest differences in cell voltage ΔU_{max} were calculated at each current density point for each lab for two temperatures (60 °C and 80 °C). Fig. 8 shows the deviations for the uncorrected performance measurements and Fig. 9 the deviations for the iR-corrected values.

Fig. 8 shows the uncorrected voltage deviation for all labs at 60 °C and 80 °C. For 60 °C, the highest deviation for all current densities is found for Lab 3 (light blue curve in Fig. 8). For 80 °C, the highest deviation depends on the current density and for the small current density as well as the 2.5 A*cm^2 is found at Lab 3 (dark blue curve in Fig. 8) and for values between 0.5 A*cm^2 and 2 A*cm^2 is found at Lab 2 (dark green curve, partially hidden in Fig. 8). Fig. 8 can be regarded as one of the major outcomes of the presented contribution. It shows differences in uncorrected cell voltage of ΔU_{max}(60 °C) from 0 to 12 mV and of ΔU_{max}(80 °C) from 0 to 11 mV.

These values must be taken as the reference value for the across-sites comparison, as the best achievement one can hope for is to bring down the across-sites reproducibility to the same value as the in-house reproducibility.

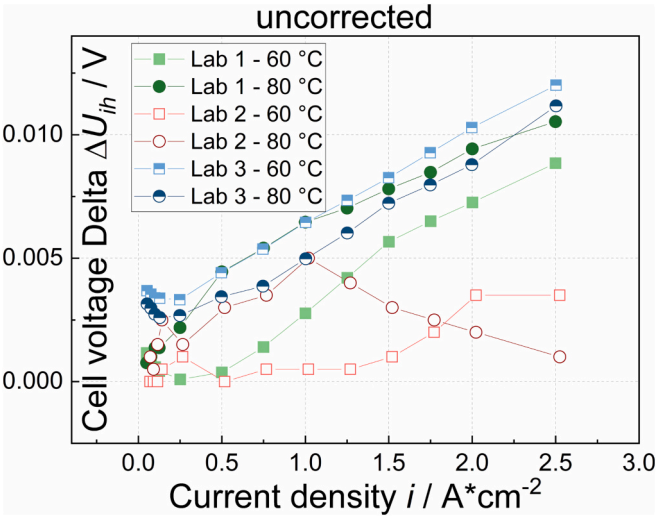

Fig. 8. Cell voltage differences from uncorrected polarization data for each lab at 60 °C and 80 °C.

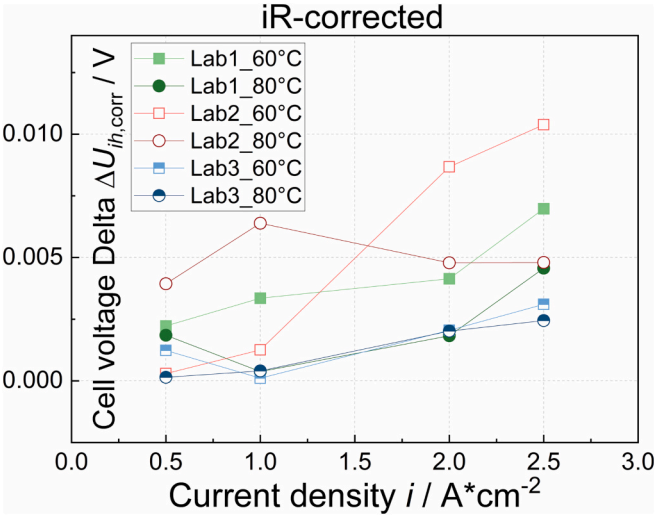

Fig. 9. Cell voltage differences from iR-corrected polarization data for each lab at 60 °C and 80 °C.

Also noticeable is the fact that Lab 1 and Lab 3 show similar and higher values than Lab 2, whose reproducibility, however, is higher, especially at higher current densities and for the lower temperature. This means, with the herein described test setup and cell components, it is possible to reach an in-house reproducibility of 5 mV and lower, which are extremely precise measurements. As 95% of all data points are below $\Delta U_{ih} = 10$ mV, all measurements that obtain results with significantly higher differences, the implementation precision (the protocol run) must be checked carefully.

In case of the iR-corrected values differences are in the same range as for the uncorrected values. It is interesting to see, however, that the deviations for Lab 2 are the highest, now, while they were the lowest for the uncorrected values. Values of up to $\Delta U_{ih,corr} = 11$ mV are quantified. 96% of all data points are below 10 mV, 91% are below 7 mV. It is noteworthy that the remaining iR-corrected deviations are similarly high as the uncorrected ones. This suggests that influences leading to differences, can counteract each other. Taking one influence out (in the actual case the ohmic losses), the remaining differences (from kinetic losses and maybe upcoming mass transport losses) can still be as high. Moreover, it is noticeable that differences in kinetics are lower for

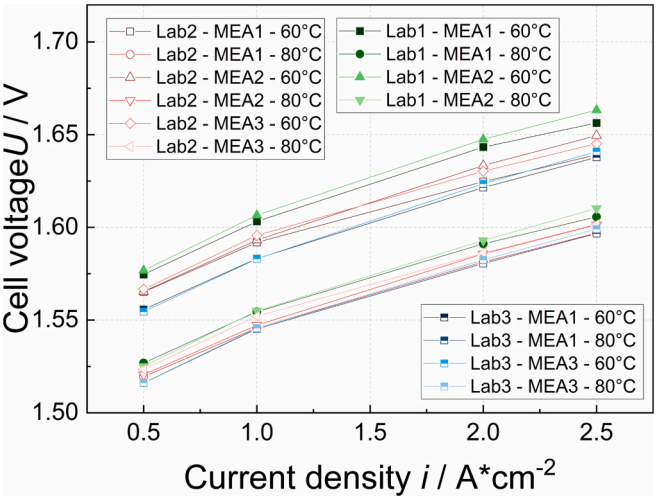

Fig. 10. iR-corrected polarization data for each lab at 60 °C and 80 °C.

higher temperatures. This can be seen clearly in Fig. 10, showing the iR-corrected polarization curves for all labs at $T = 60$ °C and 80 °C. Furthermore, Lab 1 shows the highest iR-corrected voltages, Lab 3 the lowest and Lab 2 is in between. This order compensates the differences in the HFRs (ohmic losses), which show values in reverse order (see Fig. 7).

4.2. Across-sites reproducibility

The above discussed in-house reproducibility is the necessary basis to understand data comparisons of different institutions. The main objective of this publication is the quantification of the voltage differences that can be expected when different institutions compare data, even if the same test protocol and the same materials were used (to the possible extent). In the following, the differences between these institutions (called lab differences, ΔU_{labs}) are analyzed based on the same polarization and impedance data. First, the differences in transient behavior during conditioning are shown and discussed, followed by the polarization data and the calculated lab differences in uncorrected and iR-corrected state. Fig. 11 shows the transient behavior of all cell assemblies during the last step of conditioning (potentiostatic step at $U =$ 1.7 V). As a MEA is only used once, the abbreviation "MEA" when referring to measured results is used as synonym for "cell assembly" throughout this article. In general, a lab specific transient behavior can be observed: At Lab 1 currents decrease with time, whereas at Lab 3, current increase, both with different, lab specific, slopes. The behavior at Lab 2 is different in such a way that the current density first drops and then significantly increases after roughly five hours and after that flattens off, showing the highest changes in current densities of all Labs. A current density increase of 302 mA*cm^{-2} is seen, whereas a current density decrease of 129 mA*cm^{-2} is observed for Lab 1. At the end of the conditioning procedure differences are getting smaller and curves from all three lab converge towards a current density window of 106 mA*cm^{-2}, which is – especially taking the similarity of the polarization curves reported in Section 4.1 into account – still surprisingly high. For all institutions that want to compare their data to the herein presented data, it is highly recommended to check if their data lies within this expectation window (grey bar), and make sure to take the Vi's out of the second run. Otherwise, comparability to the data reported here cannot be guaranteed.

Fig. 12 shows mean polarization curves from up and down curves for each lab. For quantification of the voltage differences, again, the delta between the highest and lowest voltage points for each current density was taken (from all three labs). These voltage differences are depicted in Fig. 13. The differences increased compared to the in-house differences (Fig. 8) by almost a factor of two. 96% of all data points are below a

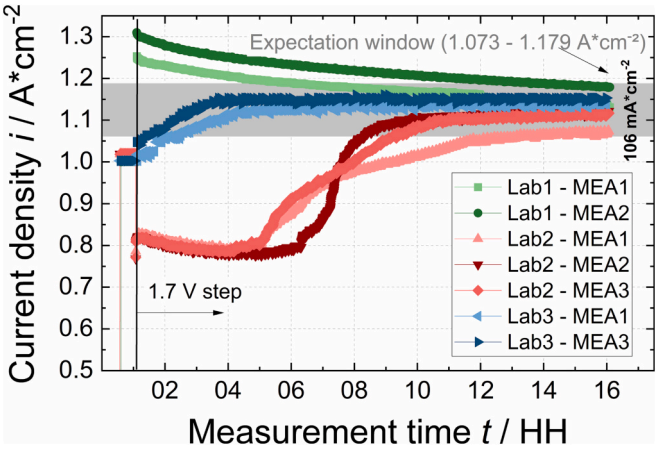

Fig. 11. Transient current density signals at the potentiostatic step (last step) during conditioning for each lab at 80 °C.

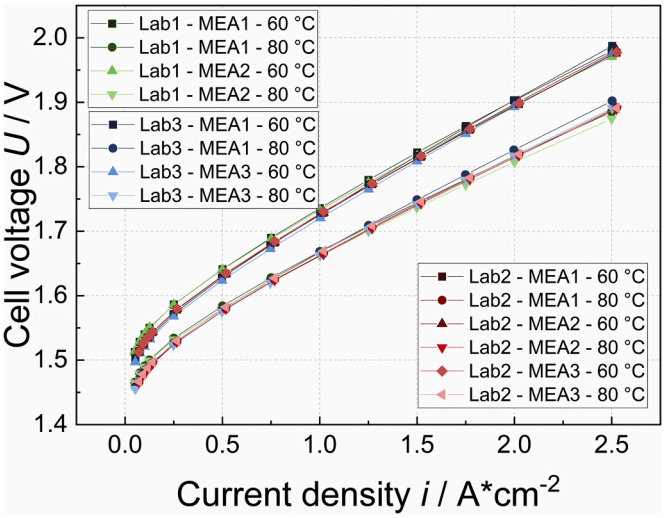

Fig. 12. Mean polarization data out of an up-down curve pair of data for each lab at 60 °C and 80 °C.

difference of $\Delta U_{labs} = 20$ mV. A clear increase at $T = 80$ °C for values above a current density of $i = 1$ A*cm^{-2} can be observed. The lowest in-house deviation is found for Lab 1, the highest deviation for Lab 3. This is, on the one hand, a reflection of the different ohmic resistances (see Fig. 7) and, on the other hand, an increasing mass transport loss for Lab 2 and Lab 3 whereas at Lab 1 this effect is not observed. This is reflected by the low frequency end of the impedance spectra at high current densities (see the impedance analysis section and especially Fig. 6).

The same data analysis process was done for the iR-corrected curves shown in Fig. 10. Like for the in-house differences, the values almost spread over the same range. Voltage differences ($\Delta U_{abs,corr}$) between 9 mV and 26 mV are quantified (see Fig. 14). The fact that the values are similarly high, shows again that the losses can counteract each other. In general, lab differences are smaller at higher temperatures. But this might change for higher current densities, which were not investigated herein.

4.3. Influence of thermal management

Temperature generally shows a high impact on any overpotential and effect in a PEM water electrolysis cell. Therefore, regulation and

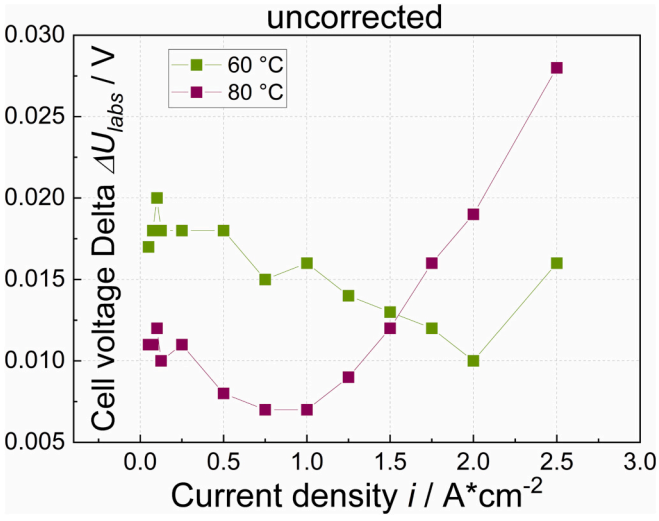

Fig. 13. Cell voltage differences when the uncorrected polarization data for all labs are unified into one data set for 60 °C and 80 °C, respectivily.

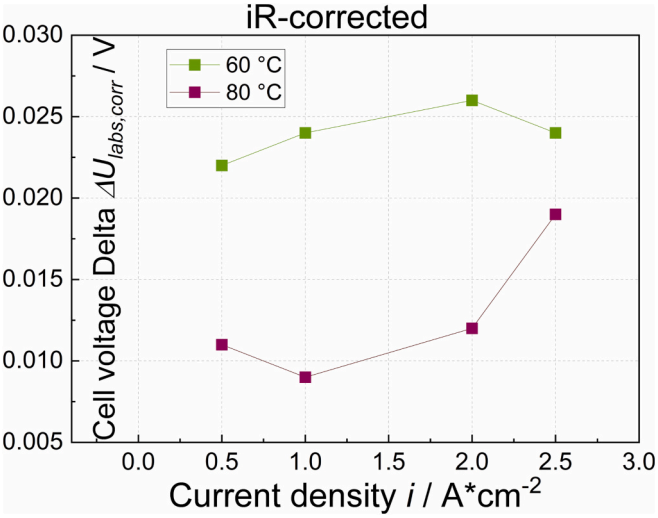

Fig. 14. Cell voltage differences when the corrected polarization data for all labs are unified into one data set for 60 °C and 80 °C, respectivily.

control of the cell temperature is crucial. This can be done in various ways. Temperature sensors can be installed differently into fittings, with different distances to the cell and at different places in the piping or even inside the cell itself. To check the influences and the differences in performance resulting from these degrees of freedom, 4 variations of thermal control were tested according to the descriptions in chapter 2.3.1. Also, a suggestion of a definition of cell temperature for the presented test cell is given in this chapter.

In Fig. 15 two representative cell assemblies (MEA 1 and MEA 2) at Lab 1 are compared. MEA 1 was tested using four different ways of thermal control (temperature control variation, T-var. 01–04, see also Section 3.2) for each run. For the second cell assembly (MEA 2), all four runs were tested with the same variation (T-var. 01). From the graphs, it can be seen, that the thermal management used shows minor differences in the electrolysis performance ($\Delta U = 7$ mV @ $i = 2.5$ A*cm^{-2} for the first runs). The difference for the second runs is slightly higher ($\Delta U = 10$ mV). These values are close to, but below the differences observed when T-variation is unchanged and defined as in-house reproducibility (see Fig. 8). This means, the changed T-variation is not increasing the voltage differences above the expected reproducibility level originating from other influences like reproducibility from the assembling procedure of the cell.

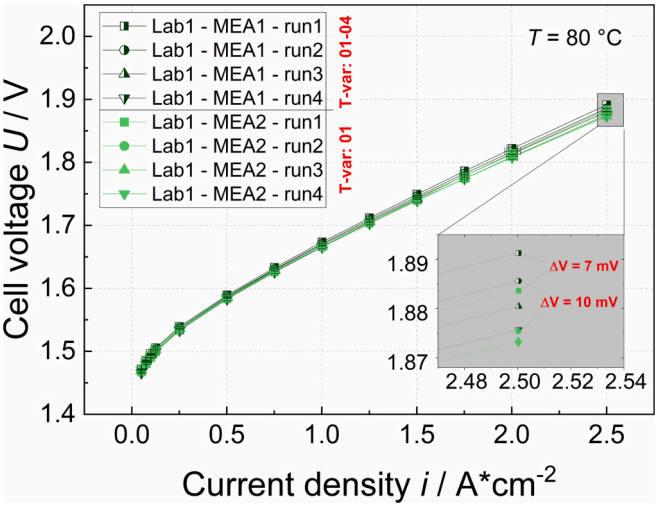

Fig. 15. Polarization curves obtained at Lab 1 for different temperature control variations. For MEA 1 (dark green), a different temperature control setting was used for each run, whereas for MEA 2 (light green), the same temperature controls setting was used for all four runs. (For interpretation of the references to colour in this figure legend, the reader is referred to the web version of this article.)

By comparing two different temperature control variations at Lab 2 in Fig. 16, it was noticed, that the first runs, show significantly higher voltage values then the other three variations. This was observed whether the temperature control was changed (MEA 1) or left unchanged (MEA 2).

For MEA 1, at $i = 2.5$ A*cm^2, a significantly higher difference between the first and the second run was obtained ($\Delta U = 48$ mV) while a similar value was obtained for MEA 2, which shows it is not T-control specific. The same effect ($\Delta U = 57$ mV) was also observed at Lab 3, see Fig. 16b. This behavior indicates that the conditioning process of the CCM is not yet fully finished during the measurements of run 1 in Lab 2 and Lab 3. It is, however, in its extend a lab specific phenomenon, as Lab 2 and Lab 3 show a rather large change after the first curve, whereas the change is significantly smaller for Lab 1. This suggests that even with a precise test protocol, differences remain in and after the presented conditioning period, as could already been seen in Fig. 11. This means on the one hand, that conditioning is not fully finished and on the other hand, remaining differences in the entire testing process significantly manifest themselves in the conditioning signals. This is regarded as one of the key learnings from the presented work, meaning that the conditioning procedure will be investigated in some more detail in the future.

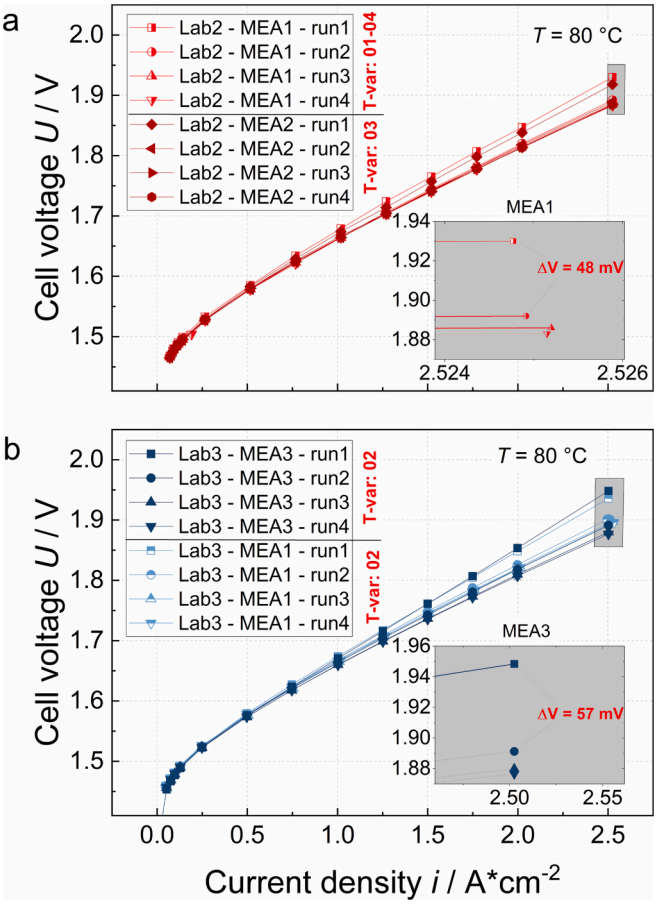

Fig. 16. Polarization curves obtained (a) at Lab 2 for different temperature control variations (light red for T-var 01–04/dark red for T-var 03 for all runs) and (b) at Lab 3 for T-var 02 for all runs (light/dark blue). Despite differences in the temperature control between the different MEAs, the first run always shows a higher voltage than runs 2–4, which is highlighted in the insets. (For interpretation of the references to colour in this figure legend, the reader is referred to the web version of this article.)

As mentioned earlier, this was the reason only the second runs (2nd *Vi*-curves) are taken into consideration for the comparison of Vi-curves at different sites. The authors conclude that the presented variations of thermal control (variations 01–04, see Section 3) do not differ much from each other in terms of performance (if the presented test cell is used). The calculated differences at $i = 2.5$ A/cm^2 originating from different thermal control variations shows values of ≈ 3 mV for those labs that tested the different variations. The influence might be higher for other test cells and other temperature control configurations.

To give the reader and the user of the test protocol an impression of the quality of thermal management at the participating labs, temperature signals during the *Vi*-curves at 80 °C for each lab with up- and down-curves for specific MEA's are depicted in Fig. 17. From the figure, differences are observable even with the same temperature control (variation 02). A rather high spread between the sensors of up to 2 K between inlet and outlet is observed for Lab 1 and Lab 3. whereas the spread is slightly lower for Lab 2.

As current densities are the same, the generated waste heat by the electrolysis process is the same at each lab. The amount of heat transported into the cell by the feed water can differ slightly as it can be seen be the inlet temperatures in Fig. 17 (anode inlet in blue, cathode inlet in red). Also, the passive heat radiation from the cell to the surrounding can be different as each lab has a specific lab environment. It can be influenced by several parameters, e.g. lab temperature in combination of the test bench ventilation, coverage of the cell as well as the three dimensional arrangements of hardware in the test bench. The observed spread of the temperature depends on the current density and decreases with an increasing amount of internal waste heat (which is partially compensating the heat radiation of the cell). This is best observed for the cathode inlet temperature (red) and cathode out temperature (violet) of Lab 1 and Lab 2 in Fig. 17: While the red curve remains stable at around 80 °C, the violet curve changes for about the same amount (~1 K). As a representative cell temperature, the authors suggest to take the arithmetic mean value out of the three anodic sensors signals (inlet, outlet and internal, see Fig. 2) This value is called T_{cell} (depicted in black in Fig. 17). Even though small differences in the transient behavior of T_{cell} can be seen, the values are close to the set temperature in all cases and very close to the temperature measured by the internal sensor on the anode side. For comparability reasons, this value should be within ±1 K around the set temperature to get to comparable data.

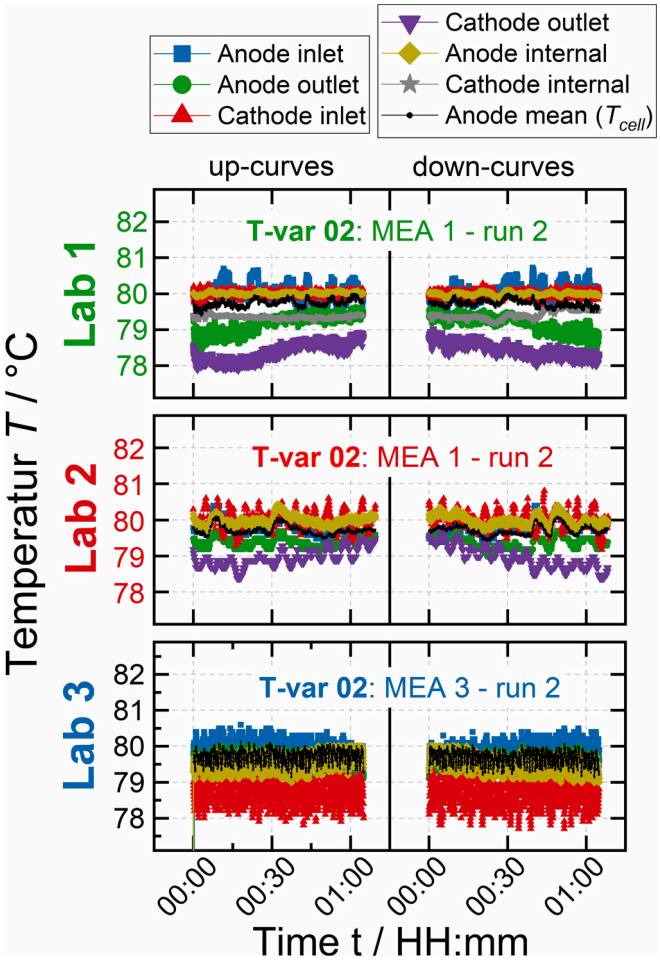

Fig. 17. Temperature signals (available sensors at each lab) over time for all threes labs (Lab 1 in green on top, Lab 2 in red in the middle and Lab 3 in blue at the bottom). Up-curves are depicted (left) as well as down-curves (right). Representative cell temperature T_{cell} is depicted in black. (For interpretation of the references to colour in this figure legend, the reader is referred to the web version of this article.)

5. Summary

The comparison of the experiments conducted at different institutions presented in this article show that a great deal of effort is required to obtain reproducible performance results across the different participating sites. The use of identical test cells and identical materials is a necessary but by no means sufficient condition.

Polarization curves obtained with the test protocol are presented for the selected reference setup of test cell and components and can be used for reproducibility purposes. The contributing authors suggest the presented test cell, test protocol, and measurement strategy to be adopted by the community to allow accurate comparison between laboratories. To achieve good across-site reproducibility, accurate application of the test protocol is crucial. Throughout more than two years of conducting this comparative study, any test interruption and deviations from the protocol had a massive impact on the performance and impedance data.

The thermal control in general is crucial for high reproducibility. The specific implementation of the tested thermal management and the tested settings, however, showed only a few millivolts of deviation. The mean values presented in this article and listed in the SI therefore, and as it is the most realistic case in scientific reality, include results from different thermal control variations. In addition, the specific and reproducible conditioning procedure of the CCM before starting the actual performance measurements proved to be highly important. This holds true despite unexpectedly large performance deviations throughout the conditioning phase. Results suggest, that despite a rather long conditioning phase (two steps at constant current, one step at constant voltage, in total 16 h), the conditioning of the CCM was not yet finished for some of the measurements. The conditioning procedure is a topic that needs further investigations and adoption to increase comparability further.

When following the measurement protocol, an across-site reproducibility of <20 mV can be obtained for uncorrected as well as iR-corrected values for current densities up to 2.5 A*cm^{-2}. This reproducibility can potentially be higher for a higher degree of harmonization of the test benches. In-house reproducibility of around 10 mV or better (< 5 mV for one of the partners) represents the upper limit that could potentially be achieved with the presented test cell and cell components. Having ruled out many harmonizable influences, mainly non-harmonizable test bench differences and production tolerances of the cell components (PTL, MEA, frames, sealings) remain as main causes for the observed performance differences.

Future work needs to include simplification of the measurement script and a change in cell components to more industrially relevant components, such as thinner titanium PTLs with protective coatings on the anode side and carbon-based PTLs on the cathode side. Also, a publicly available data base, which can be further updated with data from the community would be beneficial to increase future comparability. Based on the collated data, the effects of operating conditions on

cell degradation and lifetime (AST protocol development) can and should be investigated ultimately.

CRediT authorship contribution statement

Thomas Lickert: Supervision, Conceptualization, Writing - original draft, Writing - review & editing. **Stefanie Fischer:** Investigation, Data curation. **James L. Young:** Investigation, Formal analysis. **Selina Klose:** Investigation. **Irene Franzetti:** Investigation, Formal analysis. **Daniel Hahn:** Investigation, Formal analysis. **Zhenye Kang:** Investigation, Formal analysis. **Meital Shviro:** Supervision, Project administration. **Fabian Scheepers:** Supervision, Project administration. **Marcelo Carmo:** Project administration. **Tom Smolinka:** Project administration, Funding acquisition, Conceptualization. **Guido Bender:** Supervision, Project administration, Funding acquisition, Conceptualization. **Sebastian Metz:** Supervision, Project administration, Conceptualization, Funding acquisition, Writing - original draft, Writing - review & editing.

Declaration of Competing Interest

The authors declare that they have no known competing financial interests or personal relationships that could have appeared to influence the work reported in this paper.

Data availability

Data will be made available on request.

Acknowledgements

The authors would like to thank Dieter Hellert and Thomas Favet from the company Bekaert as well as Jan Byrknes and Armin Bayer from the company Greenerity for the good collaboration and for their permission to publish the results obtained with their products. We would like to thank Nikolai Utsch (Forschungszentrum Jülich) for his knowledgeable contributions during the revision of this article. Scientific discussions with experts from the Advanced Fuel Cells (AFC) Technology Collaboration Programme (TCP), Task 30 part of the Technology Platform of the International Energy Agency (IEA), are gratefully acknowledged. The Advanced Fuel Cells Technology Collaboration Programme covered the publication costs. Fraunhofer ISE acknowledges the funding of the Bundesministerium für Bildung und Forschung (BMBF) of the project POWER-MEE (03SF0536D), in which the used test cell was originally developed and the project HyThroughGen (03HY108B), which contributed to the development of the test protocol. This work was authored in part by the National Renewable Energy Laboratory, operated by Alliance for Sustainable Energy, LLC, for the U.S. Department of Energy (DOE) under Contract No. DE-AC36-08GO28308. Funding provided by the U.S. Department of Energy Office of Energy Efficiency and Renewable Energy (EERE) Hydrogen and Fuel Cell Technologies Office (HFTO), Award No. DE-EE0008836. The views expressed in the article do not necessarily represent the views of the DOE or the U.S. Government. The U.S. Government retains and the publisher, by accepting the article for publication, acknowledges that the U.S. Government retains a nonexclusive, paid-up, irrevocable, worldwide license to publish or reproduce the published form of this work, or allow others to do so, for U.S. Government purposes.

Appendix A. Supplementary data

Additional details of the used measurement protocol as well as the mean polarization data (uncorrected and iR-corrected) for all three labs at 60 °C and 80 °C are provided online as supplementary data at https://doi.org/10.1016/j.apenergy.2023.121898.

References

[1] Odenweller A, Ueckerdt F, Nemet GF, Jensterle M, Luderer G. Probabilistic feasibility space of scaling up green hydrogen supply. Nat Energy 2022;7(9):854–65. https://doi.org/10.1038/s41560-022-01097-4.
[2] Chatenet M, Pollet BG, Dekel DR, Dionigi F, Deseure J, Millet P, et al. Water electrolysis: from textbook knowledge to the latest scientific strategies and industrial developments. Chem Soc Rev 2022;51(11):4583–762. https://doi.org/10.1039/D0CS01079K.
[3] Grigoriev SA, Fateev VN, Bessarabov DG, Millet P. Current status, research trends, and challenges in water electrolysis science and technology. Int J Hydrogen Energy 2020;45(49):26036–58. https://doi.org/10.1016/j.ijhydene.2020.03.109.
[4] Dolci F, Gryc K, Eynard U, Georgakaki A, Letout S, Kuokkanen A, et al. Water electrolysis and hydrogen in the European Union. 2022.
[5] Gül Timur, Turk Dave, Blanco Herib, Cazzola Pierpaolo, Fukui Hiroyuki. Tae-Yoon Kim et al. The future of hydrogen: Seizing today's opportunities. Report prepared by the IEA. 2019.
[6] Carmo M, Fritz DL, Mergel J, Stolten D. A comprehensive review on PEM water electrolysis. Int J Hydrogen Energy 2013;38(12):4901–34. https://doi.org/10.1016/j.ijhydene.2013.01.151.
[7] Shiva Kumar S, Himabindu V. Hydrogen production by PEM water electrolysis – a review. Mater Sci Energy Technol 2019;2(3):442–54. https://doi.org/10.1016/j.mset.2019.03.002.
[8] Ayers K. High efficiency PEM water electrolysis: enabled by advanced catalysts, membranes, and processes. Curr Opin Chem Eng 2021;33:100719. https://doi.org/10.1016/j.coche.2021.100719.
[9] Smolinka T, Garche J, editors. Electrochemical power sources: Fundamentals, systems, and applications. Elsevier; 2022.
[10] Thomassen MS, Reksten AH, Barnett AO, Khoza T, Ayers K. Chapter 6 - PEM water electrolysis. In: Smolinka T, Garche J, editors. Electrochemical power sources: Fundamentals, systems, and applications. Elsevier; 2022. p. 199–228.
[11] Alia SM, Stariha S, Borup RL. Electrolyzer durability at low catalyst loading and with dynamic operation. J Electrochem Soc 2019;166(15):F1164. https://doi.org/10.1149/2.0231915jes.
[12] Wirkert FJ, Roth J, Jagalski S, Neuhaus P, Rost U, Brodmann M. A modular design approach for PEM electrolyser systems with homogeneous operation conditions and highly efficient heat management. Int J Hydrogen Energy 2020;45(2):1226–35. https://doi.org/10.1016/j.ijhydene.2019.03.185.
[13] Moreno Soriano R, Rojas N, Nieto E, de Guadalupe González-Huerta R, Sandoval-Pineda JM. Influence of the gasket materials on the clamping pressure distribution in a PEM water electrolyzer: bolt torques and operation mode in pre-conditioning. Int J Hydrogen Energy 2021;46(51):25944–53. https://doi.org/10.1016/j.ijhydene.2021.03.076.
[14] Fan Z, Yu H, Jiang G, Yao D, Sun S, Chi J, et al. Low precious metal loading porous transport layer coating and anode catalyst layer for proton exchange membrane water electrolysis. Int J Hydrogen Energy 2022;47(44):18963–71. https://doi.org/10.1016/j.ijhydene.2022.04.114.
[15] Salehmin MNI, Husaini T, Goh J, Sulong AB. High-pressure PEM water electrolyser: a review on challenges and mitigation strategies towards green and low-cost hydrogen production. Energ Conver Manage 2022;268:115985. https://doi.org/10.1016/j.enconman.2022.115985.
[16] Bender G, Carmo M, Smolinka T, Gago A, Danilovic N, Mueller M, et al. Initial approaches in benchmarking and round robin testing for proton exchange membrane water electrolyzers. Int J Hydrogen Energy 2019;44(18):9174–87. https://doi.org/10.1016/j.ijhydene.2019.02.074.
[17] Stähler M, Stähler A, Scheepers F, Carmo M, Stolten D. A completely slot die coated membrane electrode assembly. Int J Hydrogen Energy 2019;44(14):7053–8. https://doi.org/10.1016/j.ijhydene.2019.02.016.
[18] Ahmed KW, Jang MJ, Park MG, Chen Z, Fowler M. Effect of components and operating conditions on the performance of PEM electrolyzers: a review. Electrochem 2022;3(4):581–612. https://doi.org/10.3390/electrochem3040040.
[19] Bernt M, Schramm C, Schröter J, Gebauer C, Byrknes J, Eickes C, et al. Effect of the IrO x conductivity on the anode electrode/porous transport layer interfacial resistance in PEM water electrolyzers. J Electrochem Soc 2021;168(8):84513.
[20] Jiang G, Yu H, Li Y, Yao D, Chi J, Sun S, et al. Low-loading and highly stable membrane electrode based on an Ir@WOxNR ordered array for PEM water electrolysis. ACS Appl Mater Interfaces 2021;13(13):15073–82. https://doi.org/10.1021/acsami.0c20791.
[21] Liu C, Wippermann K, Rasinski M, Suo Y, Shviro M, Carmo M, et al. Constructing a multifunctional interface between membrane and porous transport layer for water electrolyzers. ACS Appl Mater Interfaces 2021;13(14):16182–96.
[22] Weber CC, Schuler T, de Bruycker R, Gubler L, Büchi FN, de Angelis S. On the role of porous transport layer thickness in polymer electrolyte water electrolysis. J Power Sources Adv 2022;15:100095. https://doi.org/10.1016/j.powera.2022.100095.
[23] van Pham C, Escalera-López D, Mayrhofer K, Cherevko S, Thiele S. Essentials of high performance water electrolyzers – from catalyst layer materials to electrode engineering. Adv Energy Mater 2021;11(44):2101998. https://doi.org/10.1002/aenm.202101998.
[24] Giesbrecht PK, Freund MS. Investigation of water oxidation at IrO2 electrodes in nafion-based membrane electrode assemblies using impedance spectroscopy and distribution of relaxation times analysis. J Phys Chem C 2022;126(42):17844–61. https://doi.org/10.1021/acs.jpcc.2c05104.
[25] Gollasch M, Schmeling J, Harms C, Wark M. Comparative analysis of synthesis routes for antimony-doped tin oxide-supported iridium and iridium oxide catalysts

for OER in PEM water electrolysis. Adv Mater Interfaces 2023;10(15):2300036. https://doi.org/10.1002/admi.202300036.
[26] Laube A, Hofer A, Ressel S, Chica A, Bachmann J, Struckmann T. PEM water electrolysis cells with catalyst coating by atomic layer deposition. Int J Hydrogen Energy 2021;46(79):38972–82.
[27] Bernt M, Hartig-Weiß A, Tovini MF, El-Sayed HA, Schramm C, Schröter J, et al. Current challenges in catalyst development for PEM water electrolyzers. Chem Ing Tech 2020;92(1–2):31–9. https://doi.org/10.1002/cite.201900101.
[28] Bernt M, Gasteiger HA. Influence of ionomer content in IrO 2 /TiO 2 electrodes on PEM water electrolyzer performance. J Electrochem Soc 2016;163(11):F3179–89. https://doi.org/10.1149/2.0231611jes.
[29] Yang G, Yu S, Mo J, Li Y, Kang Z, Bender G, et al. Impacts of catalyst nanolayers on water permeation and swelling of polymer electrolyte membranes. J Power Sources 2020;448:227582. https://doi.org/10.1016/j.jpowsour.2019.227582.
[30] Dedigama I, Angeli P, Ayers K, Robinson JB, Shearing PR, Tsaoulidis D, et al. In situ diagnostic techniques for characterisation of polymer electrolyte membrane water electrolysers – flow visualisation and electrochemical impedance spectroscopy. Int J Hydrogen Energy 2014;39(9):4468–82. https://doi.org/10.1016/j.ijhydene.2014.01.026.
[31] Yu H, Danilovic N, Wang Y, Willis W, Poozhikunnath A, Bonville L, et al. Nano-size IrOx catalyst of high activity and stability in PEM water electrolyzer with ultra-low iridium loading. Appl Catal Environ 2018;239:133–46. https://doi.org/10.1016/j.apcatb.2018.07.064.
[32] Liu C, Shviro M, Gago AS, Zaccarine SF, Bender G, Gazdzicki P, et al. Exploring the interface of skin-layered titanium fibers for electrochemical water splitting. Adv Energy Mater 2021;11(8):2002926. https://doi.org/10.1002/aenm.202002926.
[33] Liu L, Chen W, Li Y. An overview of the proton conductivity of nafion membranes through a statistical analysis. J Membr Sci 2016;504:1–9. https://doi.org/10.1016/j.memsci.2015.12.065.
[34] Liu C, Carmo M, Bender G, Everwand A, Lickert T, Young JL, et al. Performance enhancement of PEM electrolyzers through iridium-coated titanium porous transport layers. Electrochem Commun 2018;97:96–9. https://doi.org/10.1016/j.elecom.2018.10.021.
[35] Lettenmeier P, Kolb S, Sata N, Fallisch A, Zielke L, Thiele S, et al. Comprehensive investigation of novel pore-graded gas diffusion layers for high-performance and cost-effective proton exchange membrane electrolyzers. Energ Environ Sci 2017;10(12):2521–33. https://doi.org/10.1039/C7EE01240C.
[36] Georg Andreas, Lickert Thomas, Smolinka Tom, Zhang Xiaoling, Cooke Kevin. Corrosion protective coatings for bipolar plates and current collectors in PEM electrolysers: Novel materials and system designs for low cost, efficient and durable PEM electrolysers. In: Second international workshop on durability and degradation issues on; 2023.
[37] Bautkinova T, Utsch N, Bystron T, Lhotka M, Kohoutkova M, Shviro M, et al. Introducing titanium hydride on porous transport layer for more energy efficient water electrolysis with proton exchange membrane. J Power Sources 2023;565:232913. https://doi.org/10.1016/j.jpowsour.2023.232913.
[38] Rakousky C, Keeley GP, Wippermann K, Carmo M, Stolten D. The stability challenge on the pathway to high-current-density polymer electrolyte membrane water electrolyzers. Electrochim Acta 2018;278:324–31. https://doi.org/10.1016/j.electacta.2018.04.154.
[39] Möckl M, Ernst MF, Kornherr M, Allebrod F, Bernt M, Byrknes J, et al. Durability testing of low-iridium PEM water electrolysis membrane electrode assemblies. J Electrochem Soc 2022;169(6):64505. https://doi.org/10.1149/1945-7111/ac6d14.
[40] Torrero J, Morawietz T, García Sanchez D, Galyamin D, Retuerto M, Martin-Diaconescu V, et al. High performance and durable anode with 10-fold reduction of iridium loading for proton exchange membrane water electrolysis. Adv Energy Mater 2023;13(23):2204169. https://doi.org/10.1002/aenm.202204169.
[41] Lee JK, Schuler T, Bender G, Sabharwal M, Peng X, Weber AZ, et al. Interfacial engineering via laser ablation for high-performing PEM water electrolysis. Appl Energy 2023;336:120853. https://doi.org/10.1016/j.apenergy.2023.120853.
[42] Ayers K, Danilovic N, Harrison K, Xu H. PEM electrolysis, a forerunner for clean hydrogen. Electrochem Soc Interface 2021;30(4):67. https://doi.org/10.1149/2.F16214IF.
[43] Martin A, Trinke P, Stähler M, Stähler A, Scheepers F, Bensmann B, et al. The effect of cell compression and cathode pressure on hydrogen crossover in PEM water electrolysis. J Electrochem Soc 2022;169(1):14502. https://doi.org/10.1149/1945-7111/ac4459.
[44] Lohoff AS, Poggemann L, Carmo M, Müller M, Stolten D. Enabling high throughput screening of polymer electrolyte membrane (PEM) water electrolysis components via miniature test cells. J Electrochem Soc 2016;163(11):F3153–7. https://doi.org/10.1149/2.0211611jes.
[45] Rozain C, Millet P. Electrochemical characterization of polymer electrolyte membrane water electrolysis cells. Electrochim Acta 2014;131:160–7. https://doi.org/10.1016/j.electacta.2014.01.099.
[46] Stiber S, Balzer H, Wierhake A, Wirkert FJ, Roth J, Rost U, et al. Porous transport layers for proton exchange membrane electrolysis under extreme conditions of current density, temperature, and pressure. Adv Energy Mater 2021;11(33):2100630. https://doi.org/10.1002/aenm.202100630.
[47] Majasan JO, Cho JI, Dedigama I, Tsaoulidis D, Shearing P, Brett DJ. Two-phase flow behaviour and performance of polymer electrolyte membrane electrolysers: electrochemical and optical characterisation. Int J Hydrogen Energy 2018;43(33):15659–72. https://doi.org/10.1016/j.ijhydene.2018.07.003.
[48] Nagasawa K, Ishida T, Kashiwagi H, Sano Y, Mitsushima S. Design and characterization of compact proton exchange membrane water electrolyzer for component evaluation test. Int J Hydrogen Energy 2021. https://doi.org/10.1016/j.ijhydene.2021.08.213.
[49] Lickert T, Kiermaier ML, Bromberger K, Ghinaiya J, Metz S, Fallisch A, et al. On the influence of the anodic porous transport layer on PEM electrolysis performance at high current densities. Int J Hydrogen Energy 2020;45(11):6047–58. https://doi.org/10.1016/j.ijhydene.2019.12.204.
[50] Young JL, Kang Z, Ganci F, Madachy S, Bender G. PEM electrolyzer characterization with carbon-based hardware and material sets. Electrochem Commun 2021;124:106941. https://doi.org/10.1016/j.elecom.2021.106941.
[51] Wang W, Li K, Ding L, Yu S, Xie Z, Cullen DA, et al. Exploring the impacts of conditioning on proton exchange membrane electrolyzers by in situ visualization and electrochemistry characterization. ACS Appl Mater Interfaces 2022;14(7):9002–12. https://doi.org/10.1021/acsami.1c21849.
[52] Tomić AZ, Pivac I, Barbir F. A review of testing procedures for proton exchange membrane electrolyzer degradation. J Power Sources 2023;557:232569. https://doi.org/10.1016/j.jpowsour.2022.232569.
[53] Kuhnert E, Hacker V, Bodner M, Subramanian P. A review of accelerated stress tests for enhancing MEA durability in PEM water electrolysis cells. Int J Energy Res 2023;2023:3183108. https://doi.org/10.1155/2023/3183108.
[54] G. Tsotridis AP. EU harmonised protocols for testing of low temperature water electrolysers. 2021. https://doi.org/10.2760/58880.
[55] Frensch SH, Fouda-Onana F, Serre G, Thoby D, Araya SS, Kær SK. Influence of the operation mode on PEM water electrolysis degradation. Int J Hydrogen Energy 2019;44(57):29889–98. https://doi.org/10.1016/j.ijhydene.2019.09.169.
[56] Kang Z, Schuler T, Chen Y, Wang M, Zhang F-Y, Bender G. Effects of interfacial contact under different operating conditions in proton exchange membrane water electrolysis. Electrochim Acta 2022;429:140942. https://doi.org/10.1016/j.electacta.2022.140942.
[57] Malkow T, Pilenga A, Tsotridis G, De Marco G. EU harmonised polarisation curve test method for low-temperature water electrolysis. Luxembourg: Publications Office of the European Union; 2018.
[58] Malkow KT, Pilenga A, Blagoeva D. EU harmonised terminology for hydrogen generated by electrolysis: An open and comprehensive compendium. 2021. https://doi.org/10.2760/732809.
[59] Siegmund D, Metz S, Peinecke V, Warner TE, Cremers C, Grevé A, et al. Crossing the valley of death: from fundamental to applied research in electrolysis. JACS Au 2021;1(5):527–35. https://doi.org/10.1021/jacsau.1c00092.
[60] Zhang L, Zhao H, Wilkinson DP, Sun X, Zhang J. Electrochemical water electrolysis: Fundamentals and technologies. CRC Press; 2020.
[61] Petrovic S, Kurzweil P, Garche J. Electrochemical energy storage: Batteries, fuel cells, and hydrogen technologies. McGraw-Hill Education; 2022.
[62] Metz S, Smolinka T, Bernäcker CI, Loos S, Rauscher T, Röntzsch L, et al. Producing hydrogen through electrolysis and other processes. In: Neugebauer R, editor. Hydrogen Technologies. Cham: Springer International Publishing; 2023. p. 203–52.
[63] Scott K. Electrochemical methods for hydrogen production. Royal Society of Chemistry; 2019.
[64] Millet P, Mbemba N, Grigoriev SA, Fateev VN, Aukauloo A, Etiévant C. Electrochemical performances of PEM water electrolysis cells and perspectives. Int J Hydrogen Energy 2011;36(6):4134–42. https://doi.org/10.1016/j.ijhydene.2010.06.105.
[65] Ito H, Maeda T, Nakano A, Takenaka H. Properties of nafion membranes under PEM water electrolysis conditions. Int J Hydrogen Energy 2011;36(17):10527–40. https://doi.org/10.1016/j.ijhydene.2011.05.127.
[66] Fuel cell technologies office multi-year research, development, and demonstration plan: Section 3.4 fuel cells. 2016.
[67] Garland N, Benjamin T, Kopasz J. DOE fuel cell program: durability technical targets and testing protocols. ECS Trans 2007;11(1):923. https://doi.org/10.1149/1.2781004.
[68] Shi Y, Lu Z, Guo L, Yan C. Fabrication of membrane electrode assemblies by direct spray catalyst on water swollen Nafion membrane for PEM water electrolysis. Int J Hydrogen Energy 2017;42(42):26183–91. https://doi.org/10.1016/j.ijhydene.2017.08.205.
[69] Garcia-Navarro JC, Schulze M, Friedrich KA. Measuring and modeling mass transport losses in proton exchange membrane water electrolyzers using electrochemical impedance spectroscopy. J Power Sources 2019;431:189–204. https://doi.org/10.1016/j.jpowsour.2019.05.027.
[70] Siracusano S, Trocino S, Briguglio N, Baglio V, Aricò AS. Electrochemical impedance spectroscopy as a diagnostic tool in polymer electrolyte membrane electrolysis. Materials 2018;11(8). https://doi.org/10.3390/ma11081368.
[71] Suermann M, Schmidt TJ, Büchi FN. Cell performance determining parameters in high pressure water electrolysis. Electrochim Acta 2016;211:989–97. https://doi.org/10.1016/j.electacta.2016.06.120.
[72] Yuan X-Z, Song C, Wang H, Zhang J. Electrochemical impedance spectroscopy in PEM fuel cells. London: Springer London; 2010.
[73] Lee CH, Banerjee R, Arbabi F, Hinebaugh J, Bazylak A. Porous transport layer related mass transport losses in polymer electrolyte membrane electrolysis: A review. In: ASME 2016 14th International conference on nanochannels, microchannels, and minichannels collocated with the ASME 2016 heat transfer Summer conference and the ASME 2016 fluids engineering division Summer meeting; Sunday; 2016. V001T07A003.
[74] Franzetti Irene, Chan Ai-Lin, Pushkarev Artem, Metz Sebastian. External effects on the high frequency EIS response of a PEM electrolysis cell. Istanbul Congress Center, Istanbul, Turkey. In: Proceedings of WHEC-2022, 23rd world hydrogen energy conference; 2022. #391.